RSC Advances

PAPER

View Article Online
View Journal | View Issue

Cite this: *RSC Adv.*, 2017, **7**, 31027

First-principles study of decomposition mechanisms of $Mg(BH_4)_2 \cdot 2NH_3$ and $LiMg(BH_4)_3 \cdot 2NH_3$

Xiaowei Chen,[ab] Renquan Li,[a] Guanglin Xia,[c] Hongsheng He,[a] Xiuqing Zhang,[a] Weidong Zou*[a] and Xubin Yu*[b]

Received 11th May 2017
Accepted 6th June 2017

DOI: 10.1039/c7ra05322c

rsc.li/rsc-advances

The decomposition mechanisms of $Mg(BH_4)_2 \cdot 2NH_3$ and $LiMg(BH_4)_3 \cdot 2NH_3$ were studied by using density functional theory calculations. Compared to that of $Mg(BH_4)_2 \cdot 2NH_3$, the incorporation of $LiBH_4$ with the formation of $LiMg(BH_4)_3 \cdot 2NH_3$ slightly increased Bader charges of B atoms, meanwhile it decreased Bader charges of N atoms. $Mg(BH_4)_2 \cdot 2NH_3$ shows a low ammonia vacancy diffusion barrier, but relatively high ammonia vacancy formation energy, which lead to a low concentration of NH_3 vacancies and limit NH_3 transportation. In contrast to that of $Mg(BH_4)_2 \cdot 2NH_3$, $LiMg(BH_4)_3 \cdot 2NH_3$ has a relatively high ammonia vacancy formation energy and diffusion barrier, which suppresses ammonia release. The incorporation of $LiBH_4$ and $Mg(BH_4)_2 \cdot 2NH_3$ does not decrease but increases the hydrogen formation barrier of $LiMg(BH_4)_3 \cdot 2NH_3$, resulting in a slight increase in the dehydrogenation peak temperature, consistent with experimental results.

Introduction

Recently, many efforts have been devoted to B–N based chemical hydrides as potential hydrogen storage materials because of their high theoretical hydrogen capacity.[1–3] For instance, ammonia borane (AB), with a high H-capacity of 19.6 wt%, is a typical B–N based hydride for chemical hydrogen storage.[1] However, upon decomposition of AB, accompanied volatile compounds of ammonia, diborane, and borazine are evolved, which lead to a reduction of dehydrogenation capacity and are fatal for fuel cell applications.[1,4] Many different approaches have been adopted to facilitate hydrogen release from AB during the last decade.[5–10] Recent studies show that the substitution of H atoms in the NH_3 unit of AB by alkali metals with the formation of single or double metal amidoborane (MAB) is an effective way to improve the dehydrogenation properties of AB in terms of the reduced H_2 release temperatures, accelerated H_2 release kinetics, and minimized borazine evolved.[5,6,11–17]

Ammine metal borohydrides (AMBs), which show favourable hydrogen storage properties competitive with ammonia borane, have been developed recently as promising materials for hydrogen storage.[18–31] However, many of these composites suffer from the release of undesirable gas of ammonia during dehydrogenation. Further experimental results show that the purity of gas released and dehydrogenation temperature of AMBs can be improved by using double-cation substitutions approach and tuning BH_4/NH_3 ration.[15,24,32,33] The experimental and theoretic studies indicate that ammonia is weakly bound to the metal cations with low electronegativity (<1.2) in AMBs, therefore tend to release ammonia at low temperature.[32,34] Although these studies have provided valuable insight for understanding the decomposition processes of single metal cation AMBs, the results may not be applicable to double cations AMBs. For instance, $Mg(BH_4)_2 \cdot 2NH_3$ (with electronegativity of 1.31 for Mg cation) mainly release hydrogen along with a small amount of ammonia.[23] The incorporation of $LiBH_4$ (with low electronegativity of 0.98 for Li cation) and $Mg(BH_4)_2 \cdot 2NH_3$ with the formation of double cations ammine borohydride, $LiMg(BH_4)_3 \cdot 2NH_3$ results in improving the purity of gas released compared to $Mg(BH_4)_2 \cdot 2NH_3$.[35] Further improved dehydrogenation of ammine magnesium borohydride by tuning the NH_3/BH_4 ratios and combining $Mg(BH_4)_2 \cdot 2NH_3$ with MgH_2 and $NaAlH_4$ were reported.[36–39]

The mixed-cation strategy offers a promising route toward tuneable dehydrogenation of ammine metal borohydrides, however, a detail study of the dehydrogenation mechanism is still needed for further improving their dehydrogenation performance. Herein, we presented a comparison study of the electronic structure and dehydrogenation mechanisms of $Mg(BH_4)_2 \cdot 2NH_3$ and $LiMg(BH_4)_3 \cdot 2NH_3$ by density functional theory (DFT) calculation.

[a]*Department of Physics, School of Science, Jimei University, Xiamen, 361021, China. E-mail: phyzwd@jmu.edu.cn*

[b]*Department of Materials Science, Fudan University, Shanghai 200433, China. E-mail: yuxuebin@fudan.edu.cn*

[c]*Institute for Superconducting and Electronic Materials, University of Wollongong, North Wollongong, NSW, Australia*

Computational method

$Mg(BH_4)_2 \cdot 2NH_3$ crystallizes in the orthorhombic structure with space group of *Pcab* and lattice parameters of $a = 17.4872(4)$ Å, $b = 9.4132(2)$ Å, $c = 8.7304(2)$ Å.[23] $LiMg(BH_4)_3 \cdot 2NH_3$ has a hexagonal structure with space group $P6_3$ and lattice constants of $a = b = 8.0002(1)$ Å and $c = 8.3944$ Å.[35] The geometric structures were optimized by DFT calculation as implemented in MedeA@VASP code.[40] To describe the weak van der Waals $H^{+}\cdots{}^{-}H$ dihydrogen bonds, the optB86b-vdW functional[41–43] was adopted for geometric optimization. Plane waves with kinetic energy cutoff of 500 eV were used. The generalized gradient approximation (GGA) of Perdew–Burke–Ernzerhof (PBE) was adapted to treat the exchange and correlation of electronics.[44,45] The projector-augmented wave (PAW) approach was used to describe the electron-ion interactions[46] with 1s2s2p of Li, s2p1 of B, s2p3 of N, s2p0 of Mg as the explicit valence electrons. The Brillouin zones were sampled by Monkhorst–Pack *k*-point meshes[47] with meshes points spacing less than 0.05 per Å for both $Mg(BH_4)_2 \cdot 2NH_3$ and $LiMg(BH_4)_3 \cdot 2NH_3$. Structural relaxations of atomic positions were carried out until the total energies and residual forces were less than 1.0×10^{-5} eV and 0.02 eV $Å^{-1}$, respectively. For the calculation of NH_3 vacancy formation energies and H_2 formation energies, $1 \times 2 \times 2$ supercells of $Mg(BH_4)_2 \cdot 2NH_3$ and $2 \times 2 \times 2$ supercells of $LiMg(BH_4)_3 \cdot 2NH_3$ were used. Our tests showed that the used of $1 \times 2 \times 2$ supercells of $Mg(BH_4)_2 \cdot 2NH_3$ and $2 \times 2 \times 2$ supercells of $LiMg(BH_4)_3 \cdot 2NH_3$ with *k*-point mesh spacing less than 0.05 per Å yield energies that converged within 0.01 eV $(f.u.)^{-1}$. The NH_3 diffusion barriers and H_2 formation barriers were estimated by using climbing image nudged elastic band (CI-NEB) method.[48,49]

The NH_3 vacancy formation energy was estimated using the following equation:

$$E_c = E_{total} - E(\text{AMBs-}NH_3) - E(NH_3)$$

where E_{total} is the total energy of the AMBs supercells; $E(NH_3)$ represents the energy of isolate NH_3 molecule; $E(\text{AMBs-}NH_3)$ is the total energy of the AMBs supercells after NH_3 molecules are removed. The positive energy of E_c indicates that the creation of NH_3 vacancy is an endothermic process; while the negative energy of E_c indicates that the creation of NH_3 vacancy is an exothermic process.

The concentration of ammonia vacancy in $Mg(BH_4)_2 \cdot 2NH_3$ and $LiMg(BH_4)_3 \cdot 2NH_3$ could be estimated by the following equation[50]

$$c = N_{sites} N_{config} \exp(E_c/kT)$$

where E_c is the formation energy of NH_3 vacancy; N_{sites} represents the number of sites that the defect can be incorporated; N_{config} is the number of configurations per site in which the vacancy can be formed; k and T represent Boltzmann constant and temperature, respectively.

Results and discussion

Electronic structure

The electron localization function (ELF) and charge transfer between the H, N, B atoms and metal cations (Li and Mg) were analysed to understand the bonding characters of $Mg(BH_4)_2 \cdot 2NH_3$ and $LiMg(BH_4)_3 \cdot 2NH_3$. The H atoms bond to N atom and B atom are represent as (N)H and (B)H, respectively. As shown in Fig. 1, the calculated ELF shows the covalent bonding of N–H and B–H. Although the Mg–H bonds are mainly ionic, the distorted ELF isosurfaces around (B)H, (N)H and Mg indicate partial covalent bond feature of Mg–H. The low ELF value around Li indicates the essentially ionic bonding character of Li–H. Table 1 shows the Bader charges of (B)H, N(H), N, B and Mg for $Mg(BH_4)_2 \cdot 2NH_3$ are −0.58/−0.64, 0.44, −1.30, 1.59 and 1.65, respectively. The Bader charge of Li is 0.90 for $LiMg(BH_4)_3 \cdot 2NH_3$, indicates a strong ionization of the Li cation. Hence, Li cation transfers most of its 2s electron to neighbouring BH_4 unit, similar to that of $LiBH_4$. Compared to $Mg(BH_4)_2 \cdot 2NH_3$, the incorporation of $LiBH_4$ with the formation of $LiMg(BH_4)_3 \cdot 2NH_3$ barely affects the charge distribution of H

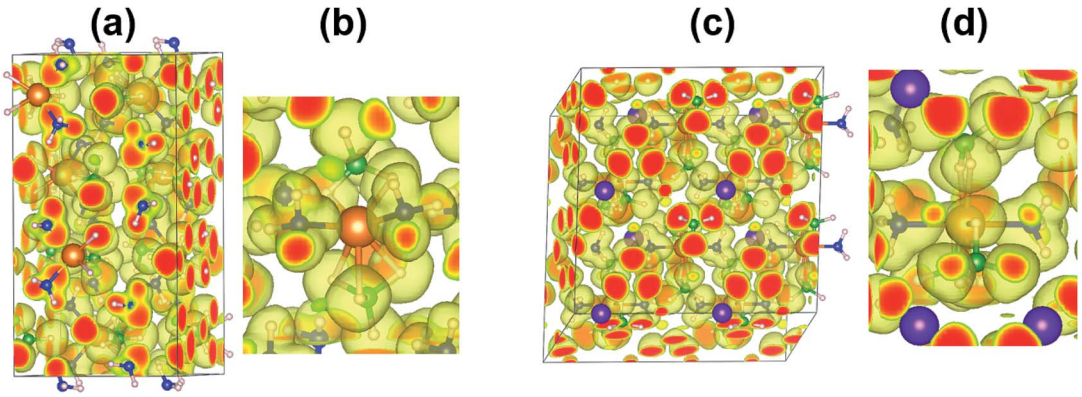

Fig. 1 The calculated electron localization function (ELF) for (a) $Mg(BH_4)_2 \cdot 2NH_3$ and (c) $LiMg(BH_4)_3 \cdot 2NH_3$ plotted as yellow-colored transparent isosurfaces at a level of 0.6; (b) and (d) present zoomed-in view showing more details for $Mg(BH_4)_2 \cdot 2NH_3$ and $LiMg(BH_4)_3 \cdot 2NH_3$, respectively. The green, pink, orange, purple and blue colors represent B, H, Mg, Li and N atoms, respectively.

Table 1 Bader charge of $Mg(BH_4)_2 \cdot 2NH_3$ and $LiMg(BH_4)_3 \cdot 2NH_3$

	Bader charge	
Atom	$Mg(BH_4)_2 \cdot 2NH_3$	$LiMg(BH_4)_3 \cdot 2NH_3$
Li	—	0.90
Mg	1.65	1.64
B	1.59	1.67
N	−1.30	−1.32/−1.34
(B)H	−0.58/−0.64	−0.63
(N)H	0.44	0.45

and Mg. The Bader charge of B is slightly increased and Bader charge of N is slightly decreased in $LiMg(BH_4)_3 \cdot 2NH_3$.

Ammonia vacancy formation energies and diffusion barriers

As demonstrated by previous report, $Mg(BH_4)_2 \cdot 2NH_3$ started to release hydrogen at temperature around 120 °C, with a maximum hydrogen release rate at 205 °C.[23] A small amount of NH_3 was released along with hydrogen evolution from $Mg(BH_4)_2 \cdot 2NH_3$. The $LiMg(BH_4)_3 \cdot 2NH_3$ shows dehydrogenation performance comparable to that of $Mg(BH_4)_2 \cdot 2NH_3$, with dehydrogenation peak located at 221 °C.[35] In addition, incorporation of $LiBH_4$ with $Mg(BH_4)_2 \cdot 2NH_3$ suppresses ammonia release.

The formation and transport properties of NH_3 vacancy are crucial to the thermodynamics and kinetics of ammonia release from AMBs. To understand the microscopic mechanisms behind the release of ammonia, the formation and diffusivity of NH_3 were studied. The NH_3 vacancy was created by directly removed a NH_3 unit from $Mg(BH_4)_2 \cdot 2NH_3$ and $LiMg(BH_4)_3 \cdot 2NH_3$.

As shown in Table 2, the calculated NH_3 removal energies are 1.81 and 1.97 eV for $Mg(BH_4)_2 \cdot 2NH_3$ and $LiMg(BH_4)_3 \cdot 2NH_3$, respectively. The relatively high NH_3 removal energies indicates that the formation of NH_3 vacancies are thermodynamics unfavourable at low temperature, resulting in low concentration of ammonia vacancy for those two composites. The high formation energy of NH_3 vacancies can attribute to the coordination bond of Mg–N and $H^{+}\cdots{}^{-}H$ dihydrogen network.

In addition to the formation energies of NH_3 vacancies, the diffusive of NH_3 vacancies is also importance for ammonia release. The diffusion paths were calculated by moving a NH_3 unit from a nearby lattice site into the vacancy. The diffusion barrier is defined as the energy difference between the saddle point and the ground state. The activation energy (Q) for self-diffusion of ammonia can be obtained by combining the calculated vacancy formation energy with the diffusion barrier. As summarized in Fig. 2 and Table 2, for $Mg(BH_4)_2 \cdot 2NH_3$, the calculated energy barrier and activation energy of ammonia diffusion are 0.26 and 2.07 eV, respectively. It should be noted that the NH_3 diffusion barrier is relatively low, the formation energy of NH_3 vacancy is the dominate term in the activation energy for ammonia diffusion. The relatively high formation energy would result in low concentration of NH_3 vacancy, which limit its transport in $Mg(BH_4)_2 \cdot 2NH_3$. This is in agreement with previous report that only a small amount of NH_3 was released during decomposition of $Mg(BH_4)_2 \cdot 2NH_3$.[23]

Table 2 Calculated NH_3 vacancy formation energies (E_c), diffusion barriers (E_b) and activation energies ($Q = E_b + E_c$) for $Mg(BH_4)_2 \cdot 2NH_3$ and $LiMg(BH_4)_3 \cdot 2NH_3$

	E_c (eV)	E_b (eV)	Q (eV)
$Mg(BH_4)_2 \cdot 2NH_3$	1.81	0.26	2.07
$LiMg(BH_4)_3 \cdot 2NH_3$	1.97	1.31	3.28

The calculated ammonia vacancy diffusion barrier and activation energy of $LiMg(BH_4)_3 \cdot 2NH_3$ are 1.31 and 3.28 eV, respectively. Compared to that of $Mg(BH_4)_2 \cdot 2NH_3$, the relatively high ammonia diffusion barrier and activation energy indicate that low concentration and mobility of ammonia vacancy in $LiMg(BH_4)_3 \cdot 2NH_3$, in inconsistent with experimental results that the dehydrogenation purity of $Mg(BH_4)_2 \cdot 2NH_3$ can be improved by introducing $LiBH_4$ with the formation of $LiMg(BH_4)_3 \cdot 2NH_3$.[35]

Hydrogen formation energies and barriers

Our previous studies suggest that the initial dehydrogenation of AMBs is achieved by combination of H atoms from NH_3 and H atoms from BH_4 groups.[51,52] Therefore, H_2 formation energies were calculated by moving one (N)H and one (B)H atom away from host N or B atom to form a hydrogen molecule with H–H distance of 0.74 Å in the supercell of AMBs. The geometry optimization was first performed by fixed the H_2 positions and relaxed the rest of the atoms, following by full relaxed all of the atoms in the supercell. In agreement with our previous studies, the formation of H_2 molecules lead to significant rearrangement of the surrounding lattice, which may result in overestimated the hydrogen formation energies. In addition, both $Mg(BH_4)_2 \cdot 2NH_3$ and $LiMg(BH_4)_3 \cdot 2NH_3$ started to release hydrogen at temperature higher than their melting point. In other word, the crystal structure of $Mg(BH_4)_2 \cdot 2NH_3$ and $LiMg(BH_4)_3 \cdot 2NH_3$ disappeared before hydrogen evolved. Therefore, we further calculated the hydrogen formation energies by using the molecule model in which two formula units of $Mg(BH_4)_2 \cdot 2NH_3$ and $LiMg(BH_4)_3 \cdot 2NH_3$ were placed in a cubic cell with lattice parameter of 20 Å.

As shown in Table 3, the calculated hydrogen formation energies by using supercell of AMBs are 0.84 and 1.22 eV for $Mg(BH_4)_2 \cdot 2NH_3$ and $LiMg(BH_4)_3 \cdot 2NH_3$, respectively. In consistent with our previous theoretical study, the dissociation of H_2 results in dramatic movement of around atoms.[51] The hydrogen formation energies calculated by molecule model are −0.11 and 0.08 eV for $Mg(BH_4)_2 \cdot 2NH_3$ and $LiMg(BH_4)_3 \cdot 2NH_3$, respectively. The combination of the (N)H and (B)H results in rearrangement of the surrounding atoms, similar with our previous report.[51] The NH_2 and BH_3 units reoriented and BH_3 units moved toward NH_2 to form NH_2–BH_3 complexes. The N–B distances reduce to 1.58 Å, indicating the formation of N–B bond during dehydrogenation, in agreement with experimental observation.[14,35] However, the lengths of Li–

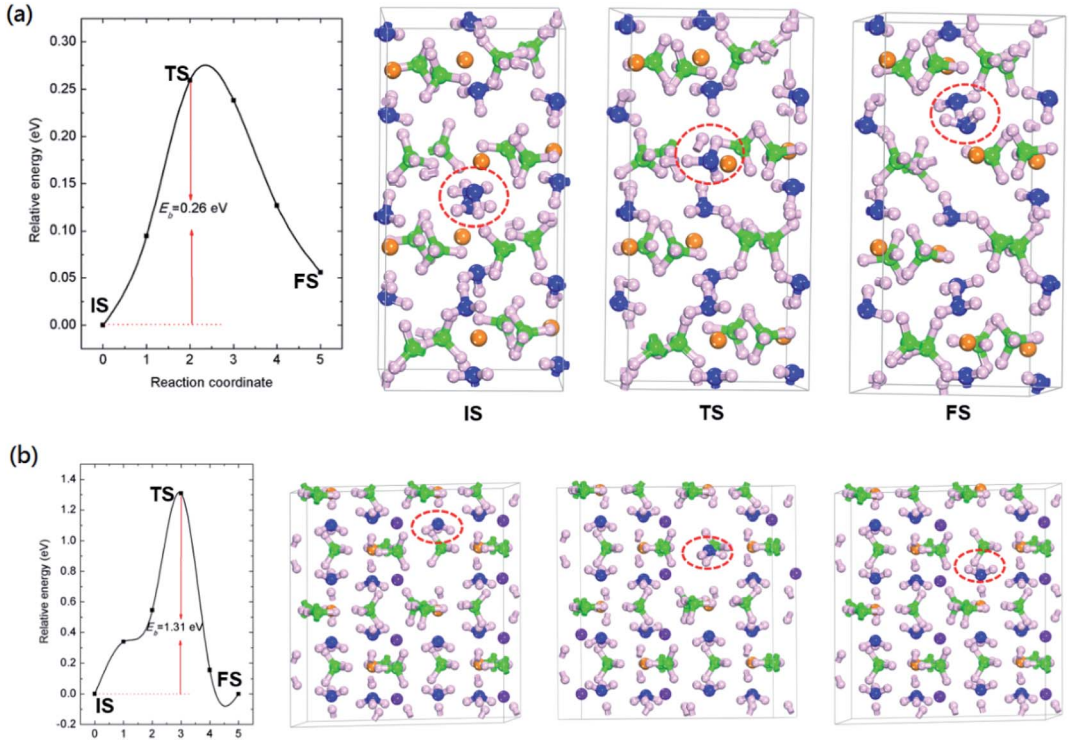

Fig. 2 The calculated energetic profiles, initial (IS), transition (TS) and final (FS) geometric structure of NH_3 diffusion for (a) $Mg(BH_4)_2 \cdot 2NH_3$ and (b) $LiMg(BH_4)_3 \cdot 2NH_3$. E_b represents the calculated energy barrier. The green, pink, orange, purple and blue colors represent B, H, Mg, Li and N atoms, respectively.

Table 3 Formation energies of H_2 release *via* (N)H and (B)H combination by using crystal model ($E_{H_2\text{-}C}$) and molecule model ($E_{H_2\text{-}M}$)

	$E_{H_2\text{-}C}$ (eV)	$E_{H_2\text{-}M}$ (eV)
$Mg(BH_4)_2 \cdot 2NH_3$	0.84	−0.11
$LiMg(BH_4)_3 \cdot 2NH_3$	1.22	0.08

N, Mg–N, B–H and N–H bonds keep almost the same after structural rearrangements.

The low H_2 formation energies of $Mg(BH_4)_2 \cdot 2NH_3$ and $LiMg(BH_4)_3 \cdot 2NH_3$ suggest that the formation of hydrogen is thermodynamic favourable at low temperature. Therefore, the energy barrier of H_2 formation is the key of those two composites release hydrogen at temperature above 100 °C.

We further calculated the energy barriers of H_2 formation and the results were summarized in Fig. 3. The calculated energy barrier of H_2 formation from $Mg(BH_4)_2 \cdot 2NH_3$ is 2.20 eV. The transition geometric structure of hydrogen release from $Mg(BH_4)_2 \cdot 2NH_3$ (Fig. 3(a)) shows the broken of B–H and N–H bonds with the formation of H_2 molecule. The H_2 molecule is located between NH_2 and BH_3 units with H_2–NH_2 and H_2–BH_3 distances of 2.47 and 2.31 Å, respectively. Meanwhile, the NH_2 unit move toward Mg cation and lead to slightly reduce the Mg–N distance from 2.16 to 1.95 Å. The calculated hydrogen formation energy barrier of $LiMg(BH_4)_3 \cdot 2NH_3$ is 2.55 eV, which is 0.35 eV higher than that of $Mg(BH_4)_2 \cdot 2NH_3$. Previous experimental results show dehydrogenation peak of 205 °C and 221 °C for $Mg(BH_4)_2 \cdot 2NH_3$ and $LiMg(BH_4)_3 \cdot 2NH_3$, respectively.[23,35] The relatively high dehydrogenation peak of $LiMg(BH_4)_3 \cdot 2NH_3$ can be attributed to the high hydrogen formation barrier. The transition geometric structure of hydrogen release from $LiMg(BH_4)_3 \cdot 2NH_3$ is similar to that of $Mg(BH_4)_2 \cdot 2NH_3$. The H_2 molecule is located between NH_2 and BH_3 unit. The H_2–NH_2 distance in transition structure of $LiMg(BH_4)_3 \cdot 2NH_3$ is 2.24 Å, which is 0.23 Å shorter than that in $Mg(BH_4)_2 \cdot 2NH_3$. And the H_2–BH_3 distance in transition structure of $LiMg(BH_4)_3 \cdot 2NH_3$ is 2.11 Å, which is 0.20 Å shorter than that in $Mg(BH_4)_2 \cdot 2NH_3$. In addition, the NH_2 unit shortening its distance to the Mg cation from 2.19 to 1.95 Å, similar to that of $Mg(BH_4)_2 \cdot 2NH_3$.

Although the above calculations show a low NH_3 diffusion barrier for $Mg(BH_4)_2 \cdot 2NH_3$, the formation energy of NH_3 vacancy is relatively high, which results in low concentration of NH_3 vacancy in $Mg(BH_4)_2 \cdot 2NH_3$. Therefore, the $Mg(BH_4)_2 \cdot 2NH_3$ mainly releases hydrogen accompany with a small amount of ammonia during decomposition. In contrast to that of $Mg(BH_4)_2 \cdot 2NH_3$, $LiMg(BH_4)_3 \cdot 2NH_3$ shows relatively high formation energy and diffusion barrier of NH_3 vacancy, which limit both the concentration and transport of ammonia, therefore improve the dehydrogenation purity. The calculated hydrogen formation barrier of $LiMg(BH_4)_3 \cdot 2NH_3$ is slightly higher than that of $Mg(BH_4)_2 \cdot 2NH_3$, therefore incorporation of $LiBH_4$ with $Mg(BH_4)_2 \cdot 2NH_3$ may not decrease the dehydrogenation temperature.

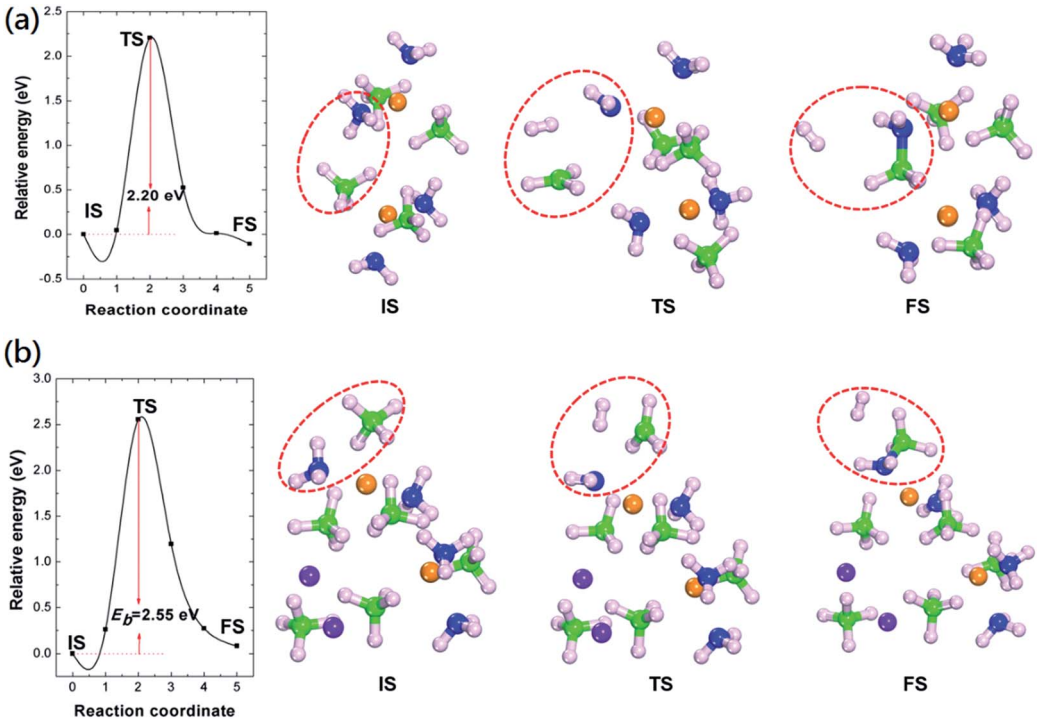

Fig. 3 The calculated energetic profiles, initial (IS), transition (TS) and final (FS) geometric structure of H_2 formation for (a) $Mg(BH_4)_2 \cdot 2NH_3$ and (b) $LiMg(BH_4)_3 \cdot 2NH_3$. E_b represents the calculated energy barrier. The green, pink, orange, purple and blue colours represent B, H, Mg, Li and N atoms, respectively.

Conclusions

First-principles calculations based on density functional theory were carried out to investigate the decomposition mechanisms of $Mg(BH_4)_2 \cdot 2NH_3$ and $LiMg(BH_4)_3 \cdot 2NH_3$. The electronic structure analysis indicates that Mg–H interaction in those two composites are mainly ionic with partial covalent bond feature. The incorporation of $LiBH_4$ and $Mg(BH_4)_2 \cdot 2NH_3$ with the formation of $LiMg(BH_4)_3 \cdot 2NH_3$ barely affects the charge distribution of H and Mg. The Bader charge of B is slightly increased and Bader charge of N decreased due to the incorporation of $LiBH_4$. Although the NH_3 diffusion barrier for $Mg(BH_4)_2 \cdot 2NH_3$ is low, the relatively high formation energy of NH_3 vacancy lead to low concentration of NH_3 vacancy and limit its transportation, in agreement with experimental results that $Mg(BH_4)_2 \cdot 2NH_3$ mainly releases hydrogen along with a small amount of ammonia. The $LiMg(BH_4)_3 \cdot 2NH_3$ shows relatively high ammonia vacancy formation energy and diffusion barrier, which suppress ammonia release compared to $Mg(BH_4)_2 \cdot 2NH_3$. The incorporation of $LiBH_4$ and $Mg(BH_4)_2 \cdot 2NH_3$ does not decrease the hydrogen formation barriers, instead slightly increase the hydrogen formation barriers of $LiMg(BH_4)_3 \cdot 2NH_3$, in agreement with experimental results that $LiMg(BH_4)_3 \cdot 2NH_3$ shows a dehydrogenation peak slightly higher than that of $Mg(BH_4)_2 \cdot 2NH_3$.

Acknowledgements

This work is supported by the National Science Fund for Distinguished Young Scholars (51625102), National Natural Science Foundation of China (51601068, 11605073) and Natural Science Foundation of Fujian Province (2016J05129, 2017J05009).

Notes and references

1 A. Staubitz, A. P. M. Robertson and I. Manners, *Chem. Rev.*, 2010, **110**, 4079–4124.
2 C. W. Hamilton, R. T. Baker, A. Staubitz and I. Manners, *Chem. Soc. Rev.*, 2009, **38**, 279–293.
3 Z. Xiong, C. K. Yong, G. Wu, P. Chen, W. Shaw, A. Karkamkar, T. Autrey, M. O. Jones, S. R. Johnson and P. P. Edwards, *Nat. Mater.*, 2008, **7**, 138–141.
4 T. B. Marder, *Angew. Chem., Int. Ed.*, 2007, **46**, 8116–8118.
5 L. Li, X. Yao, C. Sun, A. Du, L. Cheng, Z. Zhu, C. Yu, J. Zou, S. C. Smith and P. Wang, *Adv. Funct. Mater.*, 2009, **19**, 265–271.
6 X. Kang, Z. Fang, L. Kong, H. Cheng, X. Yao, G. Lu and P. Wang, *Adv. Mater.*, 2008, **20**, 2756–2759.
7 A. Paul and C. B. Musgrave, *Angew. Chem., Int. Ed.*, 2007, **119**, 8301–8304.
8 W. R. H. Wright, E. R. Berkeley, L. Alden, R. T. Baker and L. G. Sneddon, *Chem. Commun.*, 2011, **47**, 3177–3179.
9 X. Kang, J. Luo, Q. Zhang and P. Wang, *Dalton Trans.*, 2011, **40**, 3799–3801.
10 B. Meredig and C. Wolverton, *Nat. Mater.*, 2012, **12**, 123–127.
11 A. Karkamkar, C. Aardahl and T. Autrey, *Mater. Matters*, 2007, **2**, 6–9.
12 H. Wu, W. Zhou, F. E. Pinkerton, M. S. Meyer, Q. Yao, S. Gadipelli, T. J. Udovic, T. Yildirim and J. J. Rush, *Chem. Commun.*, 2011, **47**, 4102–4104.

13 J. Luo, X. Kang and P. Wang, *Energy Environ. Sci.*, 2013, **6**, 1018–1025.
14 Y. S. Chua, H. Wu, W. Zhou, T. J. Udovic, G. Wu, Z. Xiong, M. W. Wong and P. Chen, *Inorg. Chem.*, 2012, **51**, 1599–1603.
15 G. Xia, Y. Tan, X. Chen, Z. Guo, H. Liu and X. Yu, *J. Mater. Chem. A*, 2013, **1**, 1810–1820.
16 J. Spielmann, G. Jansen, H. Bandmann and S. Harder, *Angew. Chem., Int. Ed.*, 2008, **120**, 6386–6391.
17 X. Chen, Y.-J. Zhao and X. Yu, *Phys. Chem. Chem. Phys.*, 2013, **15**, 893–900.
18 Y. H. Guo, X. B. Yu, W. W. Sun, D. L. Sun and W. N. Yang, *Angew. Chem., Int. Ed.*, 2011, **123**, 1119–1123.
19 Y. H. Guo, G. L. Xia, Y. Zhu, L. Gao and X. B. Yu, *Chem. Commun.*, 2010, **46**, 2599–2601.
20 P. A. Chater, W. I. David, S. R. Johnson, P. P. Edwards and P. A. Anderson, *Chem. Commun.*, 2006, 2439–2441.
21 H. Chu, G. Wu, Z. Xiong, J. Guo, T. He and P. Chen, *Chem. Mater.*, 2010, **22**, 6021–6028.
22 F. Yuan, Q. F. Gu, X. W. Chen, Y. B. Tan, Y. H. Guo and X. B. Yu, *Chem. Mater.*, 2012, **24**, 3370–3379.
23 G. Soloveichik, J. H. Her, P. W. Stephens, Y. Gao, J. Rijssenbeek, M. Andrus and J. C. Zhao, *Inorg. Chem.*, 2008, **47**, 4290–4298.
24 Y. H. Guo, H. Wu, W. Zhou and X. B. Yu, *J. Am. Chem. Soc.*, 2011, **133**, 4690–4693.
25 L. H. Jepsen, M. B. Ley, R. Cerný, Y. Lee, Y. W. Cho, D. B. Ravnsbaek, F. Besenbacher, J. Skibsted and T. R. Jensen, *Inorg. Chem.*, 2015, **54**, 7402–7414.
26 K. Wang, J. Zhang and X. Lang, *Phys. Chem. Chem. Phys.*, 2016, **18**, 7015–7018.
27 J. M. Huang, L. Z. Ouyang, Q. F. Gu, X. B. Yu and M. Zhu, *Chem.–Eur. J.*, 2015, **21**, 14931–14936.
28 J. Huang, Y. Tan, J. Su, Q. Gu, R. Cerný, L. Ouyang, D. Sun, X. Yu and M. Zhu, *Chem. Commun.*, 2015, **51**, 2794–2797.
29 Y. J. Yang, Y. F. Liu, Y. Li, M. X. Gao and H. G. Pan, *J. Mater. Chem. A*, 2015, **3**, 570–578.
30 Y. Li, Y. F. Liu, X. Zhang, D. Zhou, Y. H. Lu, M. X. Gao and H. G. Pan, *J. Mater. Chem. A*, 2016, **4**, 8366–8373.
31 Y. J. Yang, Y. F. Liu, Y. Li, X. Zhang, M. X. Gao and H. G. Pan, *J. Mater. Chem. A*, 2015, **3**, 11057–11065.
32 Z. Tang, Y. Tan, H. Wu, Q. Gu, W. Zhou, C. M. Jensen and X. Yu, *Acta Mater.*, 2013, **61**, 4787–4796.
33 A. Emdadi, S. Demir, Y. Kışlak and A. Tekin, *J. Phys. Chem. C*, 2016, **120**, 13340–13350.
34 E. Welchman and T. Thonhauser, *J. Mater. Chem. A*, 2017, **5**, 4084–4092.
35 W. W. Sun, X. W. Chen, Q. F. Gu, K. S. Wallwork, Y. B. Tan, Z. W. Tang and X. B. Yu, *Chem.–Eur. J.*, 2012, **18**, 6825–6834.
36 Y. Yang, Y. Liu, Y. Li, M. Gao and H. Pan, *Chem.–Asian J.*, 2013, **8**, 476–481.
37 Y. Yang, Y. Liu, H. Wu, W. Zhou, M. Gao and H. Pan, *Phys. Chem. Chem. Phys.*, 2013, **16**, 135–143.
38 Y. Yang, Y. Liu, Y. Zhang, Y. Li, M. Gao and H. Pan, *J. Alloys Compd.*, 2014, **585**, 674–680.
39 Y. Li, Y. Liu, X. Zhang, Y. Yang, M. Gao and H. Pan, *Int. J. Hydrogen Energy*, 2016, **41**, 2788–2796.
40 G. Kresse and J. Furthmüller, *Phys. Rev. B: Condens. Matter Mater. Phys.*, 1996, **54**, 11169.
41 J. Klimes, D. R. Bowler and A. Michaelides, *Phys. Rev. B: Condens. Matter Mater. Phys.*, 2011, **83**, 195131.
42 J. Klimes, D. R. Bowler and A. Michaelides, *J. Phys.: Condens. Matter*, 2009, **22**, 022201.
43 M. Dion, H. Rydberg, E. Schroder, D. C. Langreth and B. I. Lundqvist, *Phys. Rev. Lett.*, 2004, **92**, 246401.
44 J. P. Perdew, K. Burke and M. Ernzerhof, *Phys. Rev. Lett.*, 1996, **77**, 3865–3868.
45 J. P. Perdew, K. Burke and Y. Wang, *Phys. Rev. B: Condens. Matter Mater. Phys.*, 1996, **54**, 16533–16539.
46 P. E. Blöchl, *Phys. Rev. B: Condens. Matter Mater. Phys.*, 1994, **50**, 17953.
47 H. J. Monkhorst and J. D. Pack, *Phys. Rev. B: Condens. Matter Mater. Phys.*, 1976, **13**, 5188–5192.
48 G. Henkelman, B. P. Uberuaga and H. Jónsson, *J. Chem. Phys.*, 2000, **113**, 9901–9904.
49 G. Henkelman and H. Jónsson, *J. Chem. Phys.*, 2000, **113**, 9978–9985.
50 C. G. van de Walle and J. Neugebauer, *J. Appl. Phys.*, 2004, **95**, 3851.
51 X. W. Chen and X. B. Yu, *J. Phys. Chem. C*, 2012, **116**, 11900–11906.
52 X. W. Chen, F. Yuan, Y. B. Tan, Z. W. Tang and X. B. Yu, *J. Phys. Chem. C*, 2012, **116**, 21162–21168.